Available online at www.sciencedirect.com
SCIENCE DIRECT®
Journal of Sound and Vibration 285 (2005) 121–148
JOURNAL OF SOUND AND VIBRATION
www.elsevier.com/locate/jsvi

Effect of track irregularities on initiation and evolution of rail corrugation

X.S. Jin*, Z.F. Wen, K.Y. Wang

State Key Laboratory of Traction Power, Southwest Jiaotong University, Chengdu 610031, China

Received 22 September 2003; received in revised form 13 May 2004; accepted 16 August 2004
Available online 16 December 2004

Abstract

The effect of track irregularities on rail corrugation is investigated in detail with the numerical method when a wheelset is steadily curving. The irregularities considered in the analysis include initial running surface of rail with periodically varying and different wave length, stochastic roughness on the rail running surface, and vertical uneven support stiffness of the rail due to the discrete sleeper supports. The numerical method considers a combination of Kalker's rolling contact theory with non-Hertzian to be modified, a linear frictional work model and a vertical dynamics model of railway vehicle coupled with a curved track. The model is also validated by an experiment with a full scale facility. The influence of different speeds of wheelset curving on the development of the corrugation is taken into account in the calculation. The numerical results indicate that (1) for existing of the initial corrugation of new rail with any wavelength the depth from the peak to trough of it decreases gradually with an increase of wheelset passage, but the initial corrugation evolved has a tendency to move in the rolling direction, (2) the amplitude of the initial stochastic roughness of new rail is gradually leveled out and but a corrugation with very small depth and a few fixed passing frequencies is initiated, the passing frequencies are the same as the natural frequencies of the track, and (3) the discrete rail supports by sleepers have a great influence on the formation of the corrugation.

*Corresponding author. Tel.: +86 28 87634355; fax: +86 28 87600868.
E-mail address: xsjin@home.swjtu.edu.cn (X.S. Jin).

0022-460X/$ - see front matter © 2004 Elsevier Ltd. All rights reserved.
doi:10.1016/j.jsv.2004.08.042

1. Introduction

Rail corrugation is one of the most serious problems in railway engineering. Its formation and development cause fierce vibrations of railway vehicle and track, noise and reduction of the use life of the structural parts. Sometimes serious corrugation of the rails leads to a derailment accident. Corrugations with small depth can be removed by grinding, but the rails with severe corrugation have to be replaced with new ones. The cost of grinding and replacement work is very high. Therefore, a great amount of money is spent every year by railway transportation companies on the maintenance and replacement of corrugated rails [1–4].

The phenomenon of rail corrugations has been observed and studied for over 100 years. Although much progress on the recognition of the mechanisms of initial corrugation formation and development has been made with theoretical and experimental methods, the studies on corrugation have not explained the mechanism of its initial formation perfectly, and have not formulated a united and validated mathematical model to explain the initial formation mechanism and the factors affecting the evolution of rail corrugation so far [5]. Probably such a situation should be attributed to corrugation theories developed insufficiently and many factors affecting the corrugation. Some of the factors have not been recognized at the present. In addition an important theory and its numerical method, which efficiently support researches on the corrugation, have not been completed yet, namely the theory of three-dimensional elastic–plastic bodies in rolling contact, in which the status of contact surfaces of the bodies, wear and elastic–plastic deformation of the materials and dynamic behavior can be taken into consideration simultaneously. Contradictions exist in some conclusions from the literatures on rail corrugation; even so, the understanding of corrugation mechanisms has become more and more closed. It is possible that different types of corrugation have different mechanisms and explanations. Ref. [2] gave a good identification of different types of corrugations with their different characteristics, and discussed the mechanisms of their initiation and propagation and treatments. However, no matter how rail corrugation initiates and propagates it is of much concern in the irregularities of track and railway vehicle, such as the periodical and stochastic varying of the running surfaces of wheel and rail, gaps at rails joints, scratches and shelling on the running surface, and unevenness stiffness of track due to discrete sleeper supports, uneven ballast bed, welding rails, etc. The existing and formation of the irregularities are unavoidable in railway site. When a train passes through a track with the irregularities mentioned above, a contact vibration between the wheel and rail occurs at some frequencies. The frequencies are related to the natural frequencies of the track and wheelset. The normal and tangential loads, frictional work, etc. between the wheel and rail fluctuate at the same frequencies. If so, the profiles of the rail and wheel are unevenly changed due to the removal and plastic deformation of material of the rail and wheel. If the contact vibration occurs periodically a corrugation initiates and develops easily. Refs. [6–15] investigated the influences of the initial irregularities with periodically varying on the corrugation with the numerical methods. Only the material wear of the wheel and rail was treated as the damage mechanism of rail profile. The authors of Refs. [6–13] integrated and used the rolling contact theories and the dynamics of railway vehicle and track, and a feedback loop effect between the transient structural dynamics of the vehicle and track and long-term material wear process in their studies. Up to now only the theoretical models of corrugation given by Ilias, Igeland [12,13] and Nielsen [14,15] are nonlinear.

According to the observation on site [2,16–18] the effect of discrete sleeper supports or sleeper pitch on the initiation and propagation of rail corrugation cannot be ignored. Knothe and his group investigated corrugation growth rate positioned between sleepers with the concepts of receptance and pinned–pinned mode in detail [8]. Vadillo and his colleagues examined a short pitch corrugation occurring between two sleepers, on the low rail in the sharp bends belonging to part of a specific section of a railway line in the Bilbao area, Spain [18,19]. According to the wavelength fixing mechanism of corrugation discussed in many of the papers mentioned above a wavelength of corrugation formed depends greatly on train speed. Recently Müller investigated the influence of train speed on a wavelength of corrugation [20,21]. In regard to the effect of the stochastic roughness on the contact surfaces of wheel and rail on corrugation there have been very few published papers to discuss it so far.

In order to further examine the initiation and propagation of the corrugation concerned in track irregularities with a numerical method, this paper presents a relatively complete numerical algorithm, in which Kalker's rolling contact theory of three-dimensional elastic bodies with the non-Hertzian form to be modified, a material wear model relating to the frictional work of the wheel and rail and the vertical dynamics model of railway vehicle and track are integrated. In the paper, the numerical analysis includes the evolution of the initiate corrugation with different wavelength on rail with an increase of wheelset passage, the effects of the stochastic roughness and the uneven vertical supporting stiffness of track on the initiation and propagation of rail corrugation when the wheelset curving steadily. The corrugation calculation ignores the influence of the lateral unstable motion of the vehicle and track on the normal loads between the wheels and rails. It is assumed that the lateral motion is in steady situation. Also the influence of plastic deformation of rail material on the corrugation is neglected since some difficulties exist in the numerical method and the capability of computers at the present. Through the detailed calculation and analysis it is found that some results obtained in the present paper are different from those of some published papers.

2. Wheel/rail contact geometry and creepages

Corrugations occurring on curved track and turnouts are the most serious in the railway field. A curved track with radius $R_0 = 600$ m is selected in the present numerical analysis, shown in Fig. 1. The curved track gage is 1443 mm and the type of rails laid is 60 kg/m. The nominal rolling radius of the wheelset passing the curve is $r_0 = 420$ mm, and it has a cone profile with TB-type from China. It is assumed that the lateral shift of center of the wheelset $y = 14$ mm and the yaw angle $\psi = 0.1^\circ$. When the wheelset is steadily curving the creepages of the wheels and rails are written as [22]

$$\begin{aligned}
\xi_{i1} &= \left(1 - \frac{r_i}{r_0}\right)\cos\psi + (-1)^i \frac{l_0}{R_0},\\
\xi_{i2} &= (-\sin\psi)\cos[\phi - (-1)^i \delta_i],\\
\xi_{i3} &= (-1)^i \frac{\sin\delta_i}{r_0} + (-1)^{i+1}\frac{\cos\delta_i}{R_0}.
\end{aligned} \tag{1}$$

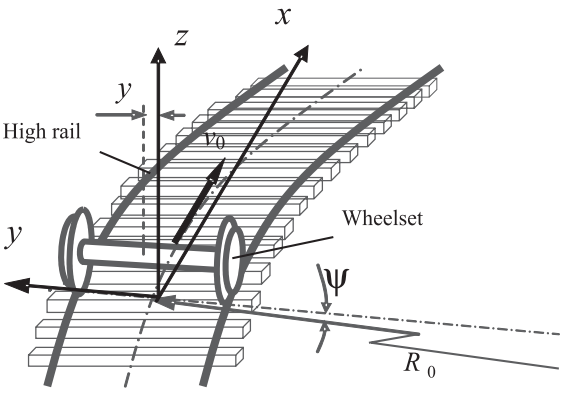

Fig. 1. A wheelset passing a curved track.

In formula (1) ξ_{i1}, ξ_{i2} and ξ_{i3} express the longitudinal, lateral and spin creepage, respectively, the sub- and superscripts $i = 1, 2$ denote the contacts of the left and right sides of the wheels and rails, respectively; l_0 is the distance between the contact points of the left and right wheels/rails when the wheelset is on the center of the track, r_i is the instant rolling radius of the left or right wheel, δ_i is the contact angle of the wheel/rail, and ϕ the rolling angle of the wheelset. The parameters of contact geometry are obtained with the numerical method discussed in Ref. [23]. So the creepages of stable curving of the wheelset are calculated with formula (1) and their values read

$$\begin{aligned} &\xi_{11} = -0.002541, \quad \xi_{12} = -0.001742, \quad \xi_{13} = -0.000124(1/\text{mm}),\\ &\xi_{21} = 0.0035, \quad \xi_{22} = -0.001743, \quad \xi_{23} = 0.000117(1/\text{mm}). \end{aligned} \tag{2}$$

3. Model of corrugation calculation

3.1. Rolling contact theory of wheel and rail

A complete calculation model of rail corrugation should consist of three parts: a dynamics model of railway vehicle coupled with a track, a theory of wheel/rail in rolling contact, and a model of material damage. Up to now Kalker's rolling contact theory of three-dimensional elastic bodies is very desirable in the analysis of rolling contact performance of wheel and rail system in elastic region [24]. Considering the influence of initial irregularity profile w_{30} and wear depth $w_{3z}^{(k)}$ after the wheel rolling passages of k times on the normal distance between the wheel and rail (as shown in Fig. 2), the discrete form of the principle of complementary virtual work of the wheel and corrugated rail in rolling contact is written as follows:

$$\begin{aligned} \min\ C = {} & \tfrac{1}{2} p_{Ii} A_{IiJj} p_{Jj} + \{[(h_J + w_{30} + w_{3J}^{(k-1)} - h_{\min}) - q] p_{J3} \\ & + (W_{J\tau} - u'_{J\tau}) p_{J\tau}\} A_0 \\ \text{s.t.:}\ & p_{J3} \geqslant 0, \quad |p_{J\tau}| \leqslant b_J, \\ & A_0 \sum_{J=1}^{M} p_{J3} = P \quad \forall \mathbf{x} \in A_c. \end{aligned} \tag{3}$$

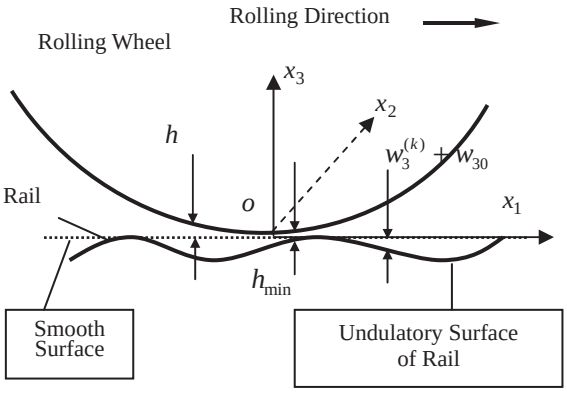

Fig. 2. Description of normal distance variation.

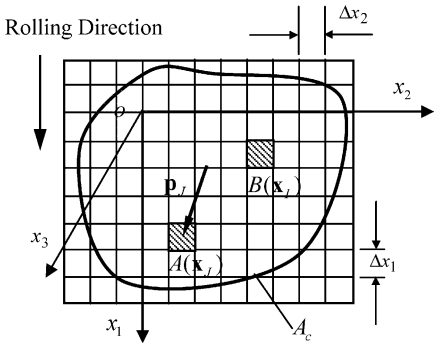

Fig. 3. Mesh covering the potential contact area.

In formula (3) subscripts $i = 1, 2, 3$ stand for the directions of x_1, x_2 and x_3 axes, respectively (see Fig. 3), $\tau = 1, 2$ denote the directions of x_1 and x_2, respectively, I, J are the numbers of the rectangular elements in the figure. A_{IiJj} is the influence coefficients of force/displacement, indicating the i direction displacement occurring at the center of rectangular element I caused by the j direction unit force acting at the center of rectangular element J. p_{Ii} is the component of traction on element I. h_J is the value of the normal gap h (shown in Fig. 2) at the center of element J, which is obtained by the calculation of contact geometry of the wheel/rail mentioned above, $w_{3J}^{(k-1)}$ is the wear depth in the x_3 direction after wheel rolling passages of $k-1$, which equals zero when the wheel rolls on the rail with smooth running surface. q is the unknown approach in the direction of x_3. u'_{J_τ} is the component of the elastic difference of the pair of contact particles at center of element J at the previous time step t', $A_0 = \Delta x_1 \times \Delta x_2 = 0.8 \times 0.8 = 0.64\,\text{mm}^2$, which is the area of the rectangular element, A_C is the potential contact area, M is the total number of the rectangular elements, selected as $21 \times 21 = 441$ in the calculation. b_J is the bound of Coulomb friction at the center of element J, which reads

$$\begin{aligned} b_J &= f p_{J3}, \quad \mathbf{x} \in H, \\ b_J &= f' p_{J3}, \quad \mathbf{x} \in S \end{aligned} \tag{4}$$

where f, f' are the static and kinetic friction coefficients of Coulomb, respectively, selected as $f = f' = 0.3$. H and S are, respectively, the stick and slip areas in the contact area. In formula (3) P, the total normal load, is written as

$$P = P_{wr} \cos \delta_i = \left(\frac{W_0}{2} + \Delta P^{(k)} \right) \cos \delta_i, \tag{5}$$

where P_{wr} is the vertical load between the wheel and the rail (see Fig. 4), W_0 is the static axle load, 21,000 kg selected in the calculation, and $\Delta P^{(k)}$ is the fluctuation of the vertical load caused by the irregularities and rail corrugation only when the wheel passage reaches k times. In formula (3), $W_{J\tau}$ $(\tau = 1, 2)$ is the component of the rigid slip between the wheel and rail at the center of element J from the previous time step t' to the present time step t, and written as

$$W_{J\tau} = \int_{t'}^{t} [\xi_{i\tau} + (-1)^{\tau} x_{3-\tau} \xi_{i3}] v_0 \, \mathrm{d}\zeta \quad (i = 1, 2, \ \tau = 1, 2). \tag{6}$$

In formula (6) ξ_{ij} $(i = 1, 2, \ j = 1, 2, 3)$ are the creepages, given by formula (1), x_1 and x_2 are the coordinates of the center of element J, v_0 is the speed of the wheel rolling, t' and t are, respectively, the previous time step and the present time step in the continuous calculation.

The Mathematical Programming Method is used to find the solution to formula (3) [24]. Also the existence and uniqueness of the solution are proved by Kalker. Therefore, $p_{Ji}, u'_{J\tau}$ $(i = 1, 2, 3, \ \tau = 1, 2, \ J = 1, 2, \ldots, 441)$ in Eqs. (3) are obtained.

3.2. Wear model of wheel and rail

A material wear model, in which loss mass of unit area is proportional to frictional work of unit area, reads [25,26]

$$\Delta m(\mathbf{x}) = C_w f_w(\mathbf{x}). \tag{7}$$

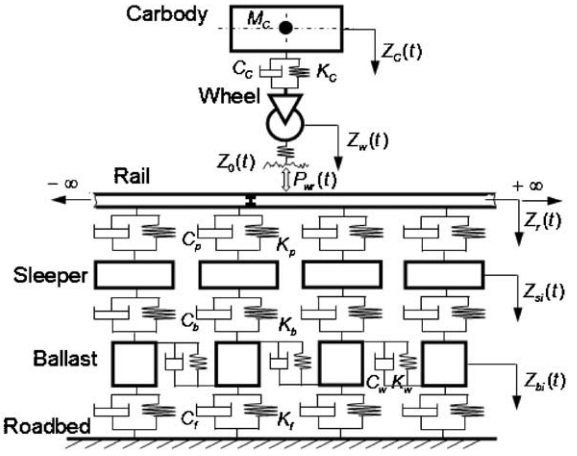

Fig. 4. Calculation model of railway vehicle and track.

In Eq. (7) $\Delta m(\mathbf{x})$ is the loss mass of unit area, $f_w(\mathbf{x})$ is the frictional work density, and C_w is the wear coefficient. Considering element J in Fig. 3, Eq. (7) is rewritten as

$$\Delta m(\mathbf{x}_J) = C_w f_w(\mathbf{x}_J) = C_w |S_{J\tau} p_{J_\tau}|. \tag{8}$$

In Eq. (8) only subscript τ is summarized. $S_{J\tau}$ reads

$$S_{J\tau} = W_{J\tau} + p_{I\tau'} A_{I\tau' J\tau} - u'_{J_\tau} \quad (\tau, \tau' = 1, 2,\ I, J = 1, 2, \ldots, 441) \tag{9}$$

which is termed the component of the total slip of the wheel and rail at the center of element J in the direction of x_τ from the previous time step t' to the present time step t. After a passage of the wheelset the depth of rail wear at the center of element J is written as

$$w_J^{(1)} = C_w |S_{J\tau} p_{J_\tau}| / \rho, \tag{10}$$

where $C_w = 1.0 \times 10^{-9}\,\mathrm{kg(N\,m)^{-1}}$ [12,14,27,29] $\rho = 7.8 \times 10^3\,\mathrm{kg/m^3}$ which is the density of the rail material. Poisson ratio and shear modulus of the material used in the calculation are, respectively, 0.3 and $7.8125 \times 10^4\,\mathrm{N/mm^2}$.

3.3. Vertical model of vehicle and track

In order to find $\Delta P^{(k)}$ caused by the irregularities and the undulatory wear, a physical model of structure of railway vehicle coupled with a track is used [28], and described in Fig. 4. In the model one quarter of a railway freight car coupled with the curved track is considered, and its lateral motion is neglected, namely the influence of the lateral fluctuation on $\Delta P^{(k)}$ is ignored since it is very small [24]. Therefore, its dynamical behaviors of the vehicle and track occur symmetrically about the central and vertical plane of the track in the longitudinal direction. Half of each sleeper is replaced with a lumped mass (M_s), the ballast is replaced with discrete lumped masses (M_b) connected with equivalent shear springs and dampers in the vertical direction. Vertical equivalent springs and dumpers are, respectively, used to connect the rail to the sleeper, the sleeper to the ballast body, and the ballast body to the roadbed. In Fig. 4, M_c is one quarter of mass of the freight car body, (K_C, C_C), (K_p, C_p), (K_b, C_b) and (K_f, C_f) are the coefficients of stiffness of equivalent springs and those of equivalent dampers, respectively, in the vertical direction, subscripts c, p, b and f indicate that the springs and dumpers are used between the car body and the wheel, the rail and the sleeper, the sleeper and the ballast, and the ballast and roadbed, respectively, (K_w, C_w) are, respectively, the stiffness coefficients of equivalent spring and that of equivalent shear damper in the vertical direction, M_s is the mass of a half of a sleeper and M_b is the equivalent mass of discrete half ballast. The structure parameters are prescribed and listed in Table 1. In the mathematical model of the structure in Fig. 4 the rail is modeled with Euler beam. The vertical deviation of the roadbed is ignored. The differential equations of the system are written as [28]

$$M_c \ddot{Z}_c + C_c(\dot{Z}_c - \dot{Z}_w) + K_c(Z_c - Z_w) = 0, \tag{11}$$

$$M_w \ddot{Z}_w + C_C(\dot{Z}_w - \dot{Z}_c) + K_c(Z_w - Z_c) - P_{wr}(t) = 0, \tag{12}$$

Table 1
Parameters of structures of vehicle and track

K_C/C_C	K_p/C_p	K_b/C_b	K_f/C_f	K_w/C_w	M_C/M_w	M_s/M_b
1.87×10^6 N/m	5.0×10^8 N/m	2.4×10^8 N/m	6.5×10^7 N/m	7.8×10^7 N/m	19.6×10^3 kg	125.5 kg
5.0×10^5 Ns/m	5.0×10^4 Ns/m	5.88×10^4 Ns/m	3.1×10^4 Ns/m	8.0×10^4 Ns/m	1.4×10^3 kg	682.6 kg

$$\ddot{q}_n(t)+\sum_{i=1}^{N}C_pY_n(x_i)\sum_{h=1}^{NM}Y_h(x_i)\dot{q}_h(t)+\frac{\mathrm{EI}}{m_r}\left(\frac{n\pi}{l}\right)^4q_n(t)+\sum_{i=1}^{N}K_pY_n(x_i)\sum_{h=1}^{NM}Y_h(x_i)q_h(t)-\sum_{i=1}^{N}C_pY_n(x_i)\dot{Z}_{si}(t)=-\sum_{i=1}^{N}K_pY_n(x_i)Z_{si}(t)+Y_n(x_P)P_{wr}(t)\quad(n=1\sim NM),\tag{13}$$

$$M_s\ddot{Z}_{si}(t)+(C_p+C_b)\dot{Z}_{si}(t)+(K_p+K_b)\dot{Z}_{si}-C_b\dot{Z}_{bi}-K_bZ_{bi}(t)-C_p\sum_{h=1}^{NM}Y_h(x_i)\dot{q}_h(t)-K_p\sum_{h=1}^{NM}Y_h(x_i)q_h(t)=0\quad(i=1\sim N),\tag{14}$$

$$M_b\ddot{Z}_{bi}(t)+(C_b+C_f+2C_w)\dot{Z}_{bi}(t)+(K_b+K_f+2K_w)Z_{bi}(t)-C_b\dot{Z}_{si}(t)-K_bZ_{si}(t)-C_w\dot{Z}_{b(i+1)}(t)-K_wZ_{b(i+1)}(t)-C_w\dot{Z}_{b(i-1)}(t)-K_wZ_{b(i-1)}(t)=0\quad(i=1\sim N),\tag{15}$$

$$Z_{b0}=\dot{Z}_{b0}=0,\qquad Z_{b(N+1)}=\dot{Z}_{b(N+1)}=0.\tag{16}$$

Eqs. (11)–(15) are the differential equations of the car-body, wheel, rail, sleeper and ballast, respectively. Eq. (16) stands for the motion equations of the equivalent ballast masses at the two ends of the calculation length of the vehicle and track dynamics. They are termed as the end conditions of system differential equations (11)–(15). If the calculation length selected is enough the effect of the end is very small. From Eq. (16) it is known that the vertical motion of the roadbed is neglected. In the equations, Z_c, Z_w, Z_s and Z_b are vertical displacements of the car-body, wheel, sleeper and ballast, respectively; those with a dot and two dots above them are the corresponding velocities and accelerations, respectively. For the fourth-order partial differential equation of Euler beam modeling the rail it is transferred the second order ordinary equations, described by Eq. (13), with Rayleigh–Ritz method, in which $Y_n(x_i)$ is the nth mode function of vertical bending of the rail, $q_n(t)$ is the generalized coordinate, $NM=100$, which is the total number of rail mode selected in the calculation, $N=100$, the number of sleeper spans, $l=0.6\times100$ m, which is the calculation length of rail, EI is the flexural rigidity of the rail and m_r the mass per unit longitudinal length, x_i $(i=1,2,\ldots,n)$ is the coordinate of the rail support point at

the sleeper, and x_P the coordinate of the contact point of the wheel and rail. $P_{wr}(t)$ is the total vertical load of the wheel and rail, and it reads

$$P_{wr}(t) = \begin{cases} C_H[Z_w - Z_r(x_P) + \delta_0 - w_{30} - w_3^{(k-1)}]^{3/2}, & Z_w - Z_r(x_P) + \delta_0 - w_{30} - w_3^{(k-1)} > 0, \\ 0, & Z_w - Z_r(x_P) + \delta_0 - w_{30} - w_3^{(k-1)} \leqslant 0. \end{cases} \quad (17)$$

It should be noted that the model of the vertical contact load (17) is approximately described with a Hertzian contact spring with a unilateral restrain. The dynamics of the vehicle is coupled with the track through Eq. (17). In Eq. (17) C_H is the coefficient of the normal contact stiffness concerning the Hertzian contact condition of the wheel and rail, selected as 1.1819×10^9 N/m, $Z_r(x_p)$ is the vertical displacement of rail at the contact point. δ_0 is the Hertzian approach between the wheel and rail caused by the static vertical load of $W_0/2$.

Eqs. (11)–(17) are those of a large scaled and nonlinear system. The stability, calculation speed and accuracy of the numerical method for the equations are very important. Zhai and his group developed two numerical methods to specially solve the coupling dynamics equations of the railway and track [30]. One is termed ''New Fast Numerical Integration for Dynamics Analysis of Large Systems'', and the other is called ''Numerical Trial Method for Determining Integration Stability to Complicate Nonlinear Problems''. In Ref. [30] the detailed discussion on the stability, calculation speed and accuracy of the two numerical methods, and also analysis of the selection of N, NM and time step size is given. The two numerical methods have been widely used in the analysis of dynamics of railway vehicle and track [28,31,32]. They are directly introduced to analyze Eqs. (11)–(17) in the present paper. Due to the limitation of paper size and the present paper interesting in the mechanism of the initiation and development of rail corrugation, the detailed discussion on the numerical methods is neglected.

For the above prescribed parameters of the track structure some natural frequencies of the track can be determined by the above-mentioned numerical methods. To that end a half of sine with a length of 30 mm and a depth of 0.01 mm is selected to model a scratch on the running surface of the rail, and used as an impulse input of the system for the simulation of a vertical dynamical response of the vehicle coupled with the track. A vertical load of the wheel and rail fluctuates at the track natural frequencies in either sides of the wheel–rail static load when the vehicle (in Fig. 4) passes the rail with the scratch. ΔP is defined as the fluctuating of the vertical load. The linear spectrum of ΔP, as shown in Fig. 5, gives the main natural frequencies of the track to be easily excited when the vehicle operates on the track. Therefore, $f_r = 118.67$ and 271.27 Hz, are, respectively, selected as the two key frequencies affecting rail corrugation in the following calculation.

3.4. Validation of corrugation model by experiment

The modified non-Hertzian rolling contact theory of Kalker is firstly used to calculate the material wear of the rail in the corrugation calculation model. It is necessary that the model is validated by experiment. The experiment on rail corrugation was carried out with a full-scale facility, as shown in Fig. 6. The experiment wheelset is real one, and the rollers have the same profile as that of real rail. The detailed description on the facility is given in Ref. [33]. In the experiment the corrugations for the many cases simulating the railway vehicle curving is

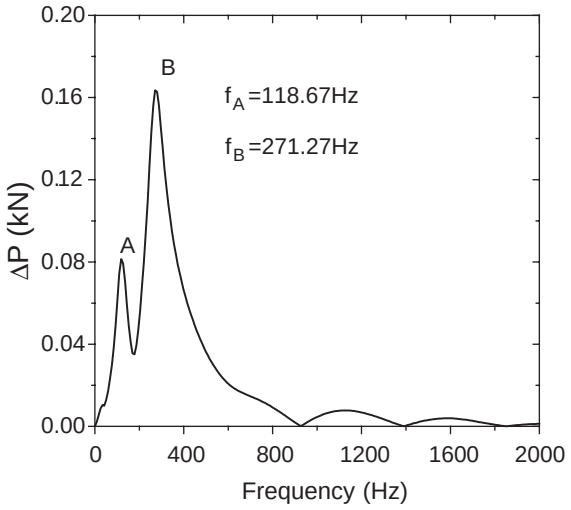

Fig. 5. Linear spectrum of vertical load fluctuation of wheel and rail.

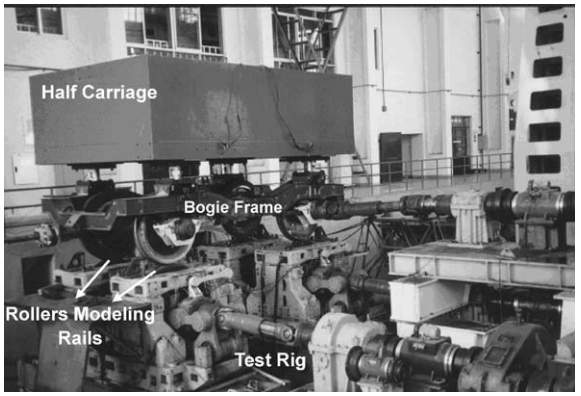

Fig. 6. A full-scale test facility for rail corrugation experiment.

reproduced on the tread of the experiment wheelset. Fig. 7(a) shows that the corrugation with about 25 mm wavelength is reproduced under the condition that the test speed is 50 km/h, the lateral shift of the wheelset center $y = 14$ mm and the yaw angle $\psi = 0^\circ$. Fig. 7(b) indicates the reproduced corrugation with about 13 mm wavelength under the test condition that the test speed is 80 km/h, $y = 0$ mm and $\psi = 0.43^\circ$. The wear patterns formed in the two test cases are quite different. In the first test case, the wheelset position set with respect to the rollers leads to the small creepages formed between the wheels and rollers, and causes the small removal of material on the wheel running surface. The contact patch presents a longer size in the rolling direction than that in the lateral direction. But in the test for Fig. 7(b), the large yaw angle, called the large attacking angle in the wheelset curving in the site, causes the large lateral creepage and the serious material wear. After a number of the wheelset turning, the wheel and the roller in rolling contact act like

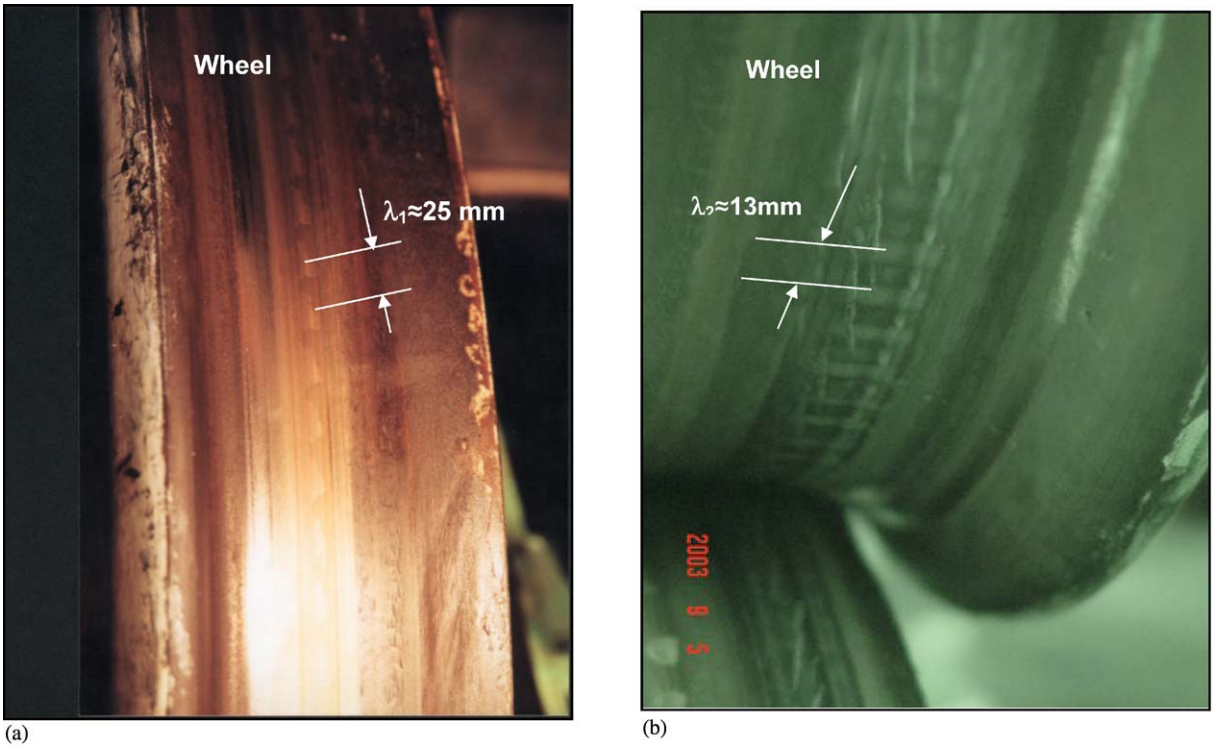

Fig. 7. (a) Reproduced corrugation for $y = 14$ mm and $\psi = 0^\circ$; (b) for $y = 0$ mm and $\psi = 0.43^\circ$.

two approximate cylinders. The contact patch formed between them has a larger size in the lateral direction than that in the rolling direction. According to the frequency-fixing mechanism of rail corrugation, the passing frequency of the corrugation in Fig. 7(a) $f_1 \approx 550$ Hz, which is obtained by dividing the test speed by λ_1. $f_2 \approx 1710$ Hz, which is the passing frequency of the corrugation shown in Fig. 7(b). Through a modal test by impulse method the natural frequencies of the test rig from 0 to 2000 Hz are obtained. Frequency response function $H_{ij}(f)$ obtained by the modal test always shows the large peaks at $f_{r1} \approx 550$ Hz and $f_{r2} \approx 1740$ Hz, respectively. So in the test of two cases, the contact vibration between the wheel and roller occurs at $f_{r1} \approx 550$ and $f_{r2} \approx 1740$. The very small lateral creep force generates between the wheel and the roller due to $\psi = 0^\circ$ in the first test case. The irregularity of the test rig causes the possible vertical contact vibration of the wheel and roller at $f_{r1} \approx 550$, namely, the vertical load of the wheel and roller oscillates at $f_{r1} \approx 550$. The amplitude of the oscillation should be small otherwise the test facility would be damaged. So far such a small oscillation of the vertical load is not obtained by measurement directly due to the problem of measurement technology. It is assumed that

$$\Delta P = 0.05 \sin(2\pi f_{r1} t)]P_0. \tag{18}$$

In Eq. (18) P_0 is the static test load. Eq. (18) indicates that the oscillating amplitude of the vertical load is 5% of the static load. In the test of the second case since $y = 0$ mm and $\psi = 0.43^\circ$ are set,

the lateral creep force between the wheel and roller is very large and the longitudinal creep force is almost zero. Therefore a possible lateral contact vibration between the wheel and roller occurs at $f_{r2} \approx 1740$. Such lateral contact vibration cannot be measured yet due to the turning of the wheel and roller during the test. It is assumed that the lateral oscillating creepage of the wheel and roller caused by the lateral contact vibration reads

$$\xi_2 = \xi_{20}[1 + 0.1\ \sin(2\pi f_{r2} t)], \tag{19}$$

where ξ_{20} is the steady lateral creepage of the wheel and roller when $y = 0$ mm and $\psi = 0.43°$. For the two test cases the steady creepages of the wheel and the roller in rolling contact are easily obtained through the contact geometry calculation [22]. Through the numerical simulation of the test of the above cases with the calculation model of corrugation discussed above, the numerical corrugation patterns, corresponding to Fig. 7(a) and (b), are indicated by Fig. 8(a) and (b), respectively. It is found that the numerical results are in good agreement with the test results. The detailed analysis on the corrugation test will takes many pages of the present paper, therefore, is neglected. In addition, it is noted that in the numerical analysis on the test Eq. (18) and Eq. (19) are used to express the coupled dynamical performance of the wheel and roller, instead of Eqs. (11)–(17). Eqs. (11)–(17) stand for the track, not for the test rig. It is very difficult as the dynamics model of the test rig is developed with finite element method. Using of any other methods to develop the dynamics model of the test rig would change its dynamical characters at the present.

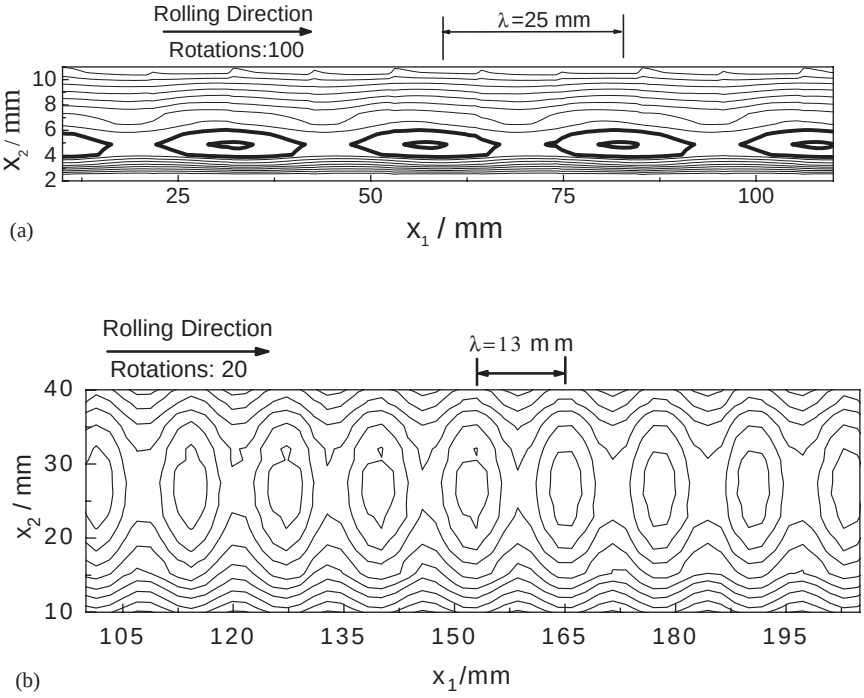

Fig. 8. Numerical corrugation pattern for: (a) Fig. 7(a); (b) for Fig. 7(b).

4. Numerical results and discussions

4.1. Effect of periodically varying of rail profile on corrugation

It is assumed that the running surface of new rail or ground rail periodically varies along the track, and the amplitude of its varying is very small. Such initial irregularity is probably caused by manufacturing or grinding of the rail. Usually the period of such varying of the rail profile is not much concerned in the dynamical characteristics of track and wheelset, and called an initial corrugation. It is assumed that the profile varying has the following function:

$$w_{30} = b_0[1 - \cos(2\pi x_1'/l_1)][1 - \cos(2\pi x_2'/l_2)] \quad |x_2'| \leqslant l_2, \tag{20}$$

where w_{30} is the variation of depth of the initial corrugation, l_1 and l_2 are the wavelength in the longitudinal and the width in lateral directions, respectively, x_1' is the coordinate of the wheel rolling distance on the rail, and $x_2' = x_2$ is the coordinate in the lateral direction, shown in Figs. 2 and 3. In the calculation, l_1 is selected to be 40, 81.92, 120 and 186.96 mm, $l_2 = 28$ mm, $b_0 = 0.0005$ mm, the running speed of the vehicle is 22.222 m/s. For the given speed the passing frequencies of the initial corrugations with 81.92 and 186.96 mm wavelengths are the same as the two main natural frequencies, as shown in Fig. 5. The passing frequencies of the other two initial corrugations are, respectively, 185.19 and 555.56 Hz. Fig. 9 indicates the evolution of the initial corrugations after the increase of wheel passage. Fig. 9(a)–(d) stands for the development situation of the corrugation with 40, 81.92, 120 and 186.96 mm wavelength, respectively. They describe only the maximum depth of the evolved corrugations from their peak to trough and their phases change. The constant wear amount of them is removed. In Fig. 9 curves 1, 2, 3 and 4 stands for the situation after the passages 1, 10, 50 and 100, respectively. Usually when a train passes through the track with corrugated rails a contact vibration between the wheel and rail occurs. If the passing frequency of the rail corrugation is the same as a natural frequency of the track, the coupling resonance of wheelset and track occurs at the natural frequency, and the situation of rail corrugation deteriorates further. But Fig. 9 shows that the depth of the corrugations from the peak to trough decreases with an increase of the wheel passage, which is in contradiction with the conclusion of the some papers published. The shorter the wavelength of the initial corrugation, the faster the decreasing rate of the corrugation depth. The same situation also occurs when the vehicle passes the corrugated rails with the passing frequency that is the same as the resonance frequency of the track, as shown in Fig. 9(b) and (d). Also it is found that the evolving corrugations have a tendency to move in the rolling direction of the wheel, which is different from some of the conclusions of Ref. [14]. Ref. [14] obtained the results according to a mechanism of rolling contact mechanics, and did not consider the feedback effect of the existing undulatory wear on the dynamical behavior of track and railway vehicle in the analysis of rail corrugation evolution. Here there are the following reasons to explain the contradictions. As it is well known, the larger the fluctuation of the vertical load between wheel and rail, the more serious the undulatory removal of rail material is under the condition of the constant creepages. When the wheel rolls over the periodically varying surface of rail (as an excitation to the wheel and rail system), the vertical load fluctuation (as a response of the system) is out of the phase of the periodically varying surface, as shown in Fig. 10. Fig. 10 illustrates the fluctuation ΔP of the vertical load when the wheel rolling over the rail with the initial corrugation of 81.92 mm

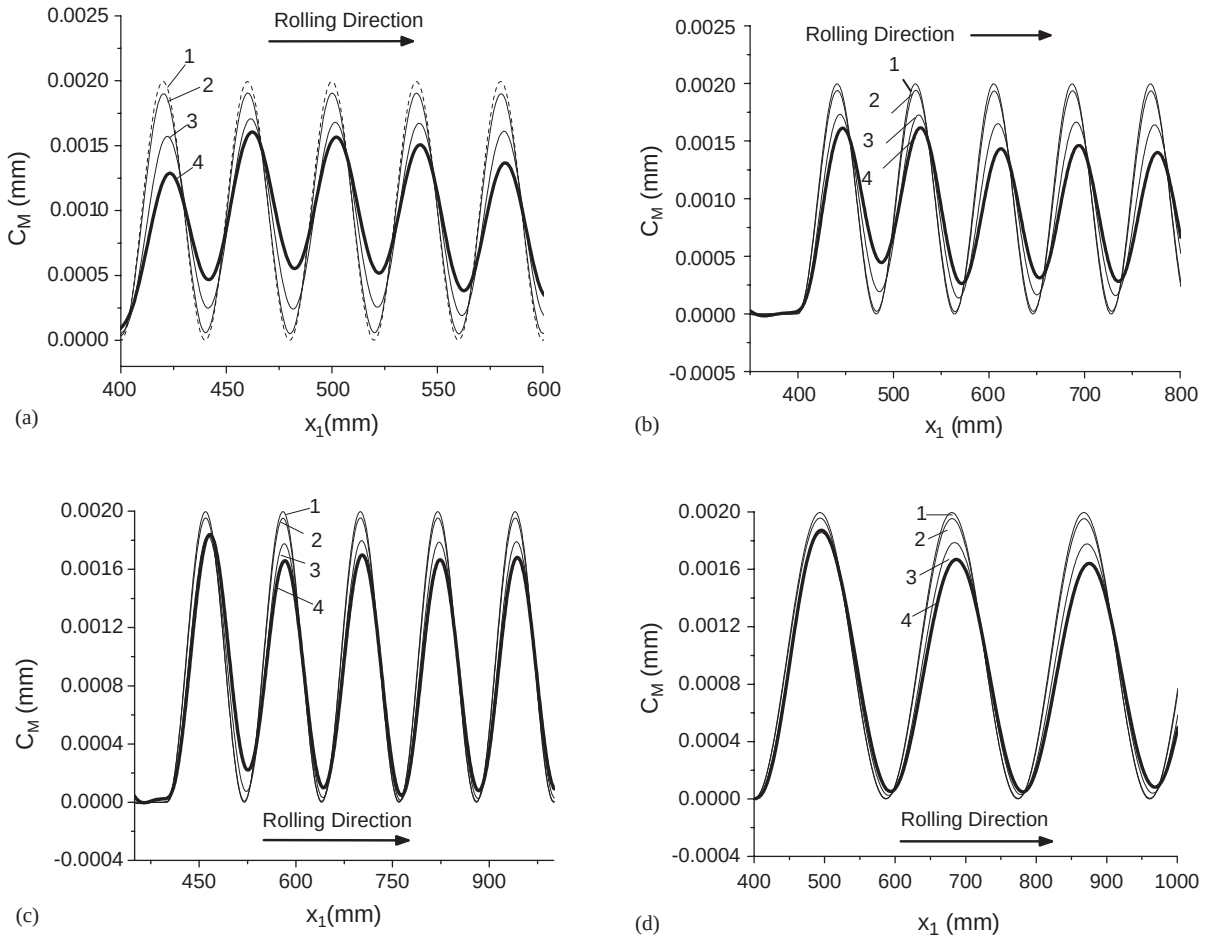

Fig. 9. Depth variation of new evolved corrugation after different number of passages: (a) 40 mm wavelength; (b) 81.92 mm wavelength; (c) 120 mm wavelength; (d) 186.96 mm wavelength.

wavelength. In Fig. 10 S_p indicates the phase difference between the fluctuation of the vertical load and the periodically varying surface. The material wear amount at the position where $\Delta P > 0$ is bigger than that at the other positions where $\Delta P < 0$. At the position with $\Delta P > 0$ the wheel just rolls uphill. That is a reason why the evolving corrugation moves little in the rolling direction. If S_p is to equal zero the initial varying surface should be leveled out quickly. But such a situation is impossible according to vibration theory. S_p depends on the rolling speed and the wave depth of the initial corrugation. As regards the research, it is not of the interesting of the present paper. It is much clear that the wave depth of the evolving corrugations decreases with an increase of the wheel passage through analyzing the change of frequency components of ΔP in the increase of wheel passage. Fig. 11 indicates the linear spectrums of ΔP during the evolution of the initial corrugation with 81.92 mm wavelength. Curve 1, 2, 3 and 4 indicate the case of 1, 10, 50 and 100 wheel passages, respectively. It is obvious that the peak height of ΔP at 271 Hz goes down and ΔP

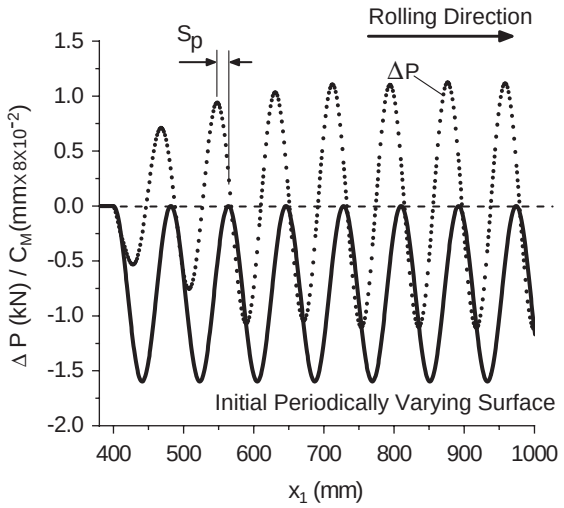

Fig. 10. Phase change between initial periodically varying surface and vertical load fluctuation.

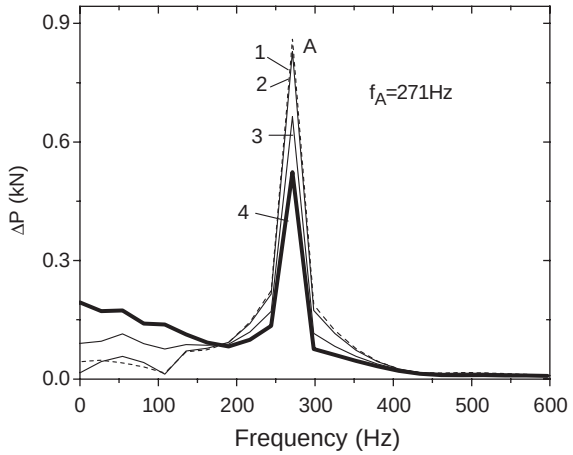

Fig. 11. Linear spectrums of ΔP for different numbers of wheel passage.

at the other frequencies, especially in the range from 0 to 271 Hz, increase with an increase of wheel passage. The periodical wear is gradually changed to an even wear. The same situation occurs in the evolution of the other initial corrugations. In Fig. 10 ΔP increases gradually and then gets into stable situation since the passing frequency of the initial corrugation is 271 Hz, which is the same as a key natural frequency of the track. Therefore a resonance between the wheel and rail occurs in short time.

Fig. 12 indicates the patterns of the corrugations evolved from the initial periodically varying surface of rail with 81.92 mm wavelength after 1, 10 and 100 passages of the wheel. The constant wear on the running surface of the rail has increasing width with an increase of the wheel passage, but the width of the undulated wear becomes gradually small. In Fig. 12(c) the pattern of the

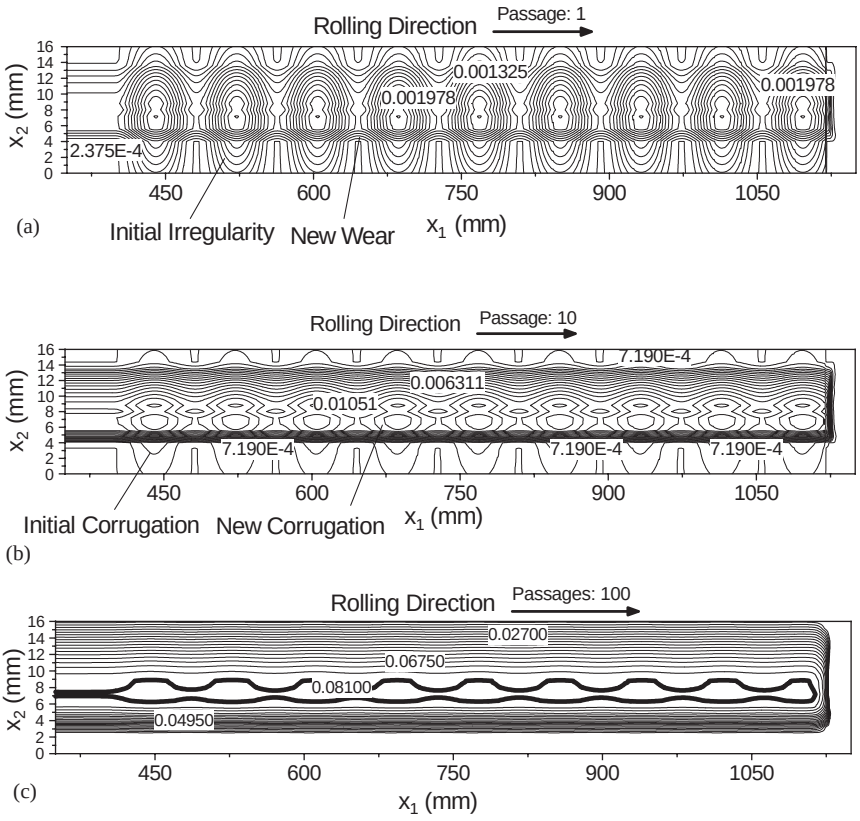

Fig. 12. Patterns of evolved corrugations after 1 passage (a), 10 passages (b), 100 passages (c).

initial corrugation cannot be seen since the new wear covers the initial corrugation and the selected interval of contour lines is not enough small to exhibit it on a same clear diagram.

4.2. *Effect of stochastic varying of rail profile on corrugation*

Micro-roughness always exists on the running surface of new rail. Usually the distribution of peaks and valleys of the roughness is stochastic. In the following analysis the analyzed area of the curved rail running surface is selected as $21\Delta x_2 \times 2500\Delta x_1 = 21 \times 2500A_0\,\mathrm{mm}^2$. $21\Delta x_2$ and $2500\Delta x_1$ are, respectively, the width and length of the analyzed area, $A_0 = \Delta x_1 \times \Delta x_2$, which is the area of a square element, as shown in Fig. 3. It is assumed that the maximum depth of the roughness from the peak to the valley is 0.005 mm, and the distribution of the peak heights is uniform in the range from 0 to 0.005 mm at the center of each square element, as illustrated by Fig. 13. In order to model the roughness function (21) is used to generate the peak values of

$$R_i = \mathrm{mod}(5R_{i-1}, 4M),$$
$$w_{30}^{(i)} = \mathrm{Int}(R_i/4) \times 10^{-7}, \tag{21}$$

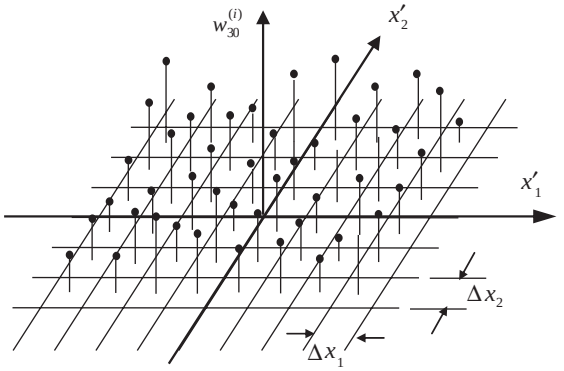

Fig. 13. Schematic illustration of stochastic roughness heights.

the stochastic roughness. In function (21) mod(...) is the modulo function, Int(...) is the integrating function, R_i is the stochastic number, $R_0 = 1.0$, which is the initial value of the stochastic numbers, also termed a seed of the stochastic numbers, $w_{30}^{(i)}$ is the peak value of the stochastic roughness, $0 \leqslant i \leqslant 21 \times 2500$, $M = 2^k$, $k = \log_2(5000 + 1) + 1$. In the generation of $w_{30}^{(i)}$, $w_{30}^{(i)}$ is recycled when $i > 50,000$. When the wheel passes the running surface with the stochastic roughness firstly, $w_{30}^{(i)}$ at the contact points along the rail running surface, is used to replace $w_0 + w_{30}^{(k)}$ in formula (17). Due to the wear, $w_{30}^{(i)}$ varies with an increase of the wheel passage. It should be stated that the step size $\Delta x_1 = 0.8$ mm, is small enough to assure the accuracy and fast convergence of the dynamic analysis of the vehicle and track [30]. But the use of the square element size, $\Delta x_1 \times \Delta x_2 = 0.8 \times 0.8\,\text{mm}^2$, is very coarse in the calculation wear under the condition of the stochastic roughness existing. So far the rolling contact theories of wheel and rail system cannot bear the responsibility for the wear calculation with micron size mesh.

Through the numerical simulation the stochastic roughness is formed on the running surface, its contour is shown in Fig. 14(a). Fig. 14(b) and (c) show the patterns of the surface wear of the rail after 10 and 50 passages of the wheel, respectively. In the wear calculation, the curving speed of the wheel is 22.222 m/s. The creepages, ξ_{11}, ξ_{12} and ξ_{13} are prescribed by formula (1), and the wheel load $W_0/2 = 102.9$ kN. After 10 passages of the wheel the wear pattern does not present some fixing wavelengths clearly, as shown in Fig. 14(b). Fig. 14(c) shows that the corrugation initiates gradually when the wheel rolls over the running surface of the rail with stochastic roughness repeatedly. It presents different wavelengths which range from 80 to 280 mm. If the lateral shift of the wheelset center varies the width of the initiated corrugation could increases.

Usually, when the wheel is rolling on the rail running surface with the stochastic roughness, the stochastic roughness excites a vibration of the wheel and the rail system with wide band frequencies. The frequencies of the vertical load fluctuation determine whether the corrugation initiates or not. In order to clear the corrugation initiation, as shown in Fig. 14, it is necessary that the linear spectrum of the fluctuation ΔP of the vertical load, caused by the stochastic roughness, is investigated. Fig. 15(a)–(d) illustrates the linear spectrum of ΔP after 1, 10, 30, 50 passages of the wheel, respectively. With an increase of the wheel passage the weight of the ingredient with frequencies larger than 400 Hz in ΔP decreases and that at frequencies ranged from 70 to 300 Hz

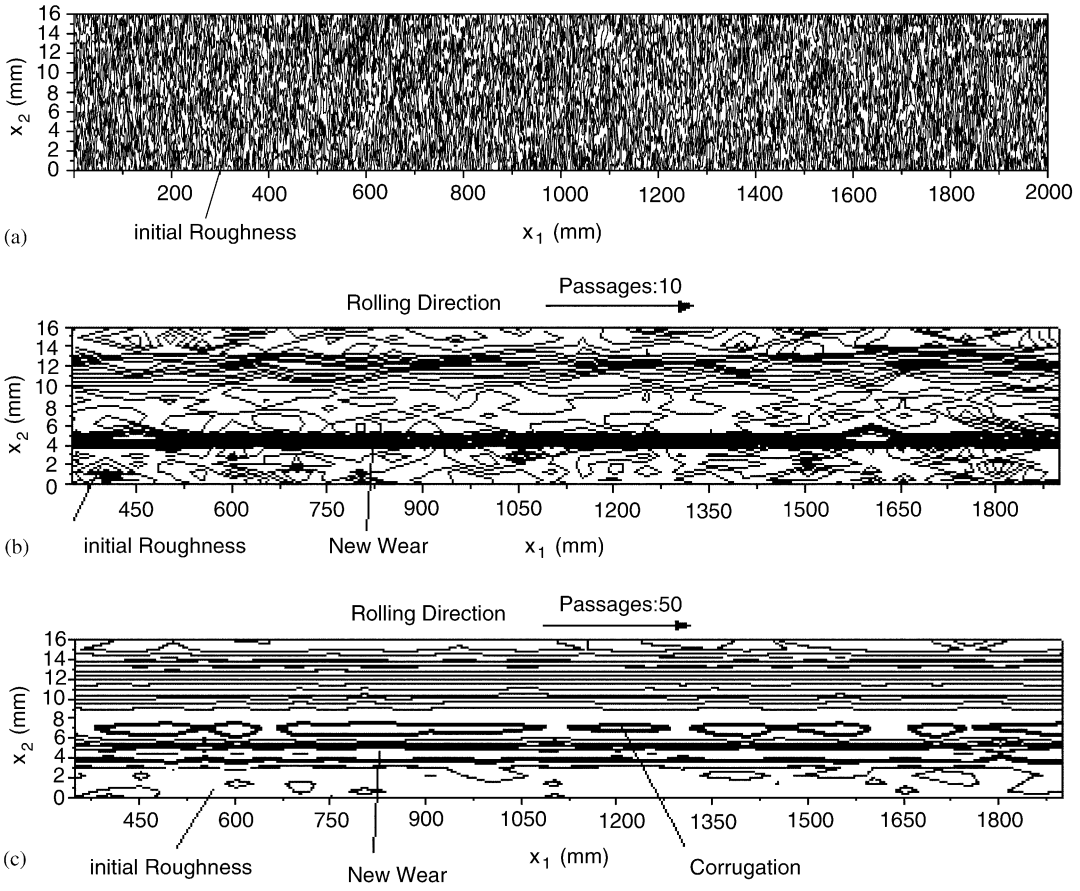

Fig. 14. Wear patterns of rail running surface with stochastic roughness: (a) Initial stochastic roughness; (b) wear after 10 passages of the wheel; (c) wear after 50 passages of the wheel.

goes up, as shown in Fig. 15(c) and (d). Such a situation leads to the occurrence of the corrugation with about 80–300 mm wavelengths (see Fig. 14). Especially the peak value of ΔP at point of 118 Hz increases rapidly with an increase of the wheel passage. As shown in Fig. 5, 118 Hz is the track natural frequency to be easily excited when the vehicle passes the track section with defects. This resonance frequency leads to about 188 mm wavelength formation. Also the peak of ΔP at 271 Hz gradually goes up with an increase of the wheel passage. Two hundred and seventy-one hertz is the other natural frequency of the track to be easily excited, as shown in Fig. 5. With the further increase of the wheel passage the two natural frequencies, 118 and 271 Hz, would play an important role in the wavelength forming of the corrugation in development. Therefore, the initiation of corrugation caused by the excitation of the initial stochastic roughness should be attributed to the wavelength-fixing mechanism.

Fig. 16 illustrates the change of the maximum wear depth of the roughness along the running surface of the rail, and curves 1, 2, 3 and 4 in the figure stands for the wear situation after the

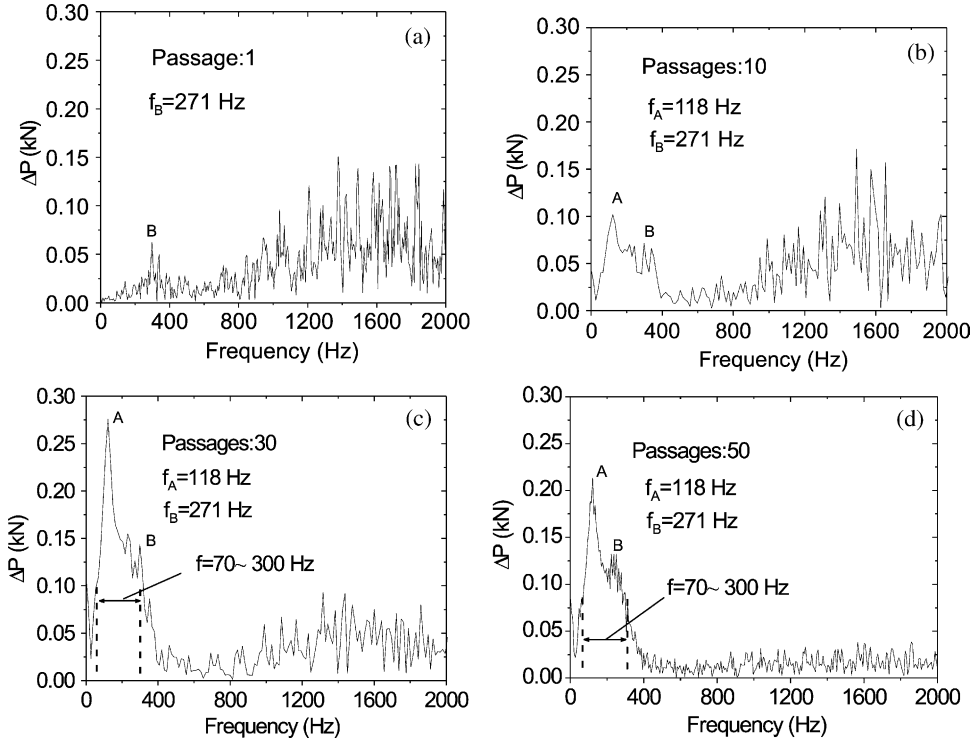

Fig. 15. Linear spectrums of ΔP after wheel passages of 1 (a), 10 (b), 30(c), 50 (d).

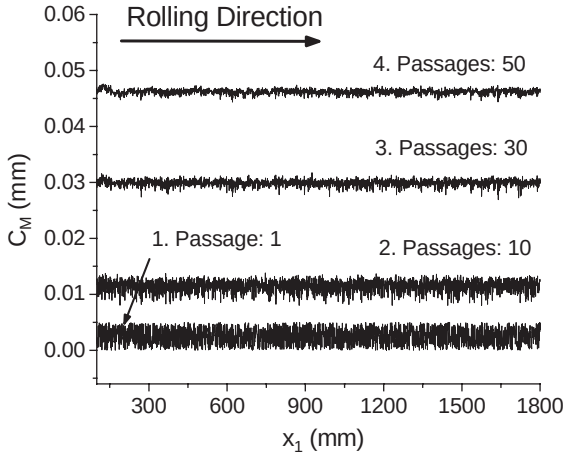

Fig. 16. Change of wear depth on rail running surface with stochastic roughness.

passages of 1, 10, 30 and 50, respectively. The peak heights of the rough surface decrease gradually, and the even wear depth on the running surface increases quickly with an increase of wheel passage. The even wear, namely the constant wear, is caused by the static vertical load and

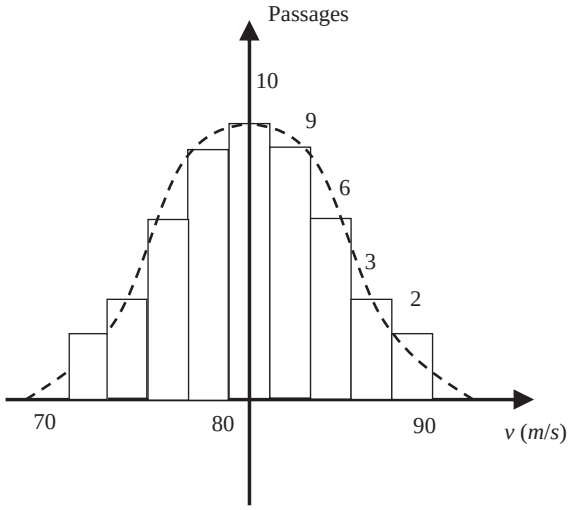

Fig. 17. Distribution of passages of train speeds.

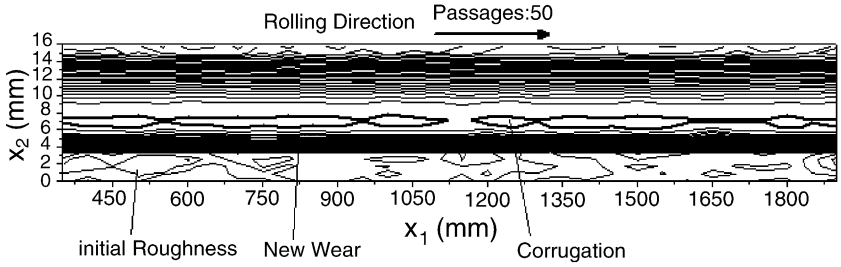

Fig. 18. Pattern of wear on running surface with initial stochastic roughness at different speed of passage.

the unsteady creepages of the wheel and the rail system. The static vertical load should be $W_0/2$. In Fig. 16, C_M includes the constant wear and the undulatory wear.

In all the cases discussed above the speeds of train curving are considered as constant. Actually, the speeds of trains passing a curved track are different any day and night. Due to the safety requirement the lowest and highest speeds of train curving is restricted for a prescribed curved track. It is assumed that 50 trains pass over the curved track every day and night, the average speed of their curving is 80 km/h, namely 22.222 m/s, the speed of the curving varies from 70 to 90 km/h, and the distribution of their speeds is an approximate normal, as shown in Fig. 17. This figure indicates that the speed range from 70 to 90 km/h is divided into nine intervals of 2.5 km/h. At each interval the number of the train passages is shown in the figure. After the trains pass the curved track at different speeds in a direction one day and night the more or less undulatory wear on the rail running surface induced by the stochastic roughness is shown in Fig. 18. Its wavelength ranges from 80 to 280 mm. If the lateral displacement of the wheelset center changes the undulation width on the running surface will increase, and the initial corrugation with very small depth probably forms in such way. By comparing Fig. 14(c) with Fig. 18 it is known that even though the running speeds of trains on the same track are different the patterns of wear have

resemblances. The wavelengths of the corrugation depend mainly on the average of train curving speeds and the main natural frequencies of track to be easily excited by an interaction of the wheel and rail.

4.3. Effect of sleeper pitch on corrugation

Since rails in a track structure is discretely supported by sleepers their vertical and lateral stiffnesses or receptances are not even, and they change periodically due to equal sleeper pitches. Sleeper pitch in special sections of a track, such curved tracks, turnouts, and some places where a hunting of train occurs, is main factor causing an occurring of corrugation. In the 80s of last century, Clark found that the short wavelength corrugation occurred only in the second half of each sleeper bay, only on high speed sections of the British Railway [17]. By theoretical analysis he also found that the vertical force of the wheel–rail contact oscillates at corrugation passing frequency in either sides of the wheel–rail static load, and the oscillation amplitude is the greatest nearby sleeper positions [16]. Knothe and his group made a detailed investigation into the material wear situation at the different positions in a sleeper bay, and found that a high corrugation growth rate occurred at the position of the rail over a sleeper. Vadillo and his colleagues found that the about 60 mm wavelength corrugation appeared at the mid-span of each sleeper bay with 1000 mm size in the Bilbao area, Spain. Through the test in which an intermediate sleeper was inserted in between each two sleepers with 1000 mm size the corrugations were ceased [18]. To explain the rare behavior they observed, Gomez and Vadillo utilized the linear model for corrugation developed by Frederick to analyze it, and demonstrated that a corrugation initially presented at the mid-span and almost disappeared above the sleeper [19,29]. In order to further investigate the effect of sleeper pitch on rail corrugation finite element method is used to analyze the vertical displacement of the track structure described by Fig. 19 under the condition of moving axle-loads of 100, 150 and 200 kN. To eliminate the influence of the end condition of finite element model the calculation length of the track to be selected covers 12 sleeper spans. It is found that the vertical displacement increases linearly with the increase of the moving static axle-load. Fig. 19

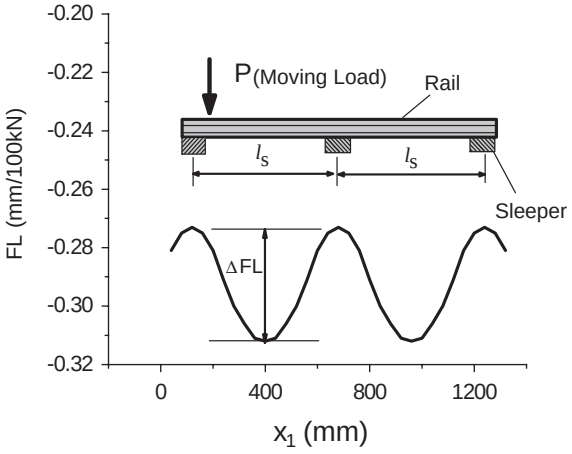

Fig. 19. Vertical static flexibility of track.

illustrates the vertical static flexible coefficient of the track. But in the dynamic model of the track discussed in Section 3.3 the effect of such vertical deformation, as shown in Fig. 19, on corrugation cannot be incarnated. In order to consider the effect we have to change formula (17) to formula (22).

$$P_{wr}(t) = \begin{cases} C_H[Z_w - Z_r(x_P) + \delta_0 - w_{30} & Z_w - Z_r(x_P) + \delta_0 - w_{30} - w_3^{(k-1)} \\ \quad -w_3^{(k-1)} - \mathrm{FL}^*(x_P)]^{3/2}, & \quad -\mathrm{FL}^*(x_P) > 0, \\ 0, & Z_w - Z_r(x_P) + \delta_0 - w_{30} - w_3^{(k-1)} \\ & \quad -\mathrm{FL}^*(x_P) \leqslant 0, \end{cases} \tag{22}$$

where $\mathrm{FL}^*(x_p)$ is the flexibility of the track under different static loads obtained by revising the curve shown in Fig. 19, and it reads

$$\mathrm{FL}^*(x_p) = \Delta\mathrm{FL}(x_p) W_0/2 \cos \delta_i. \tag{23}$$

In formula (23) the right-hand side multiplying by $\cos \delta_i$ is to consider the effect of the wheel and rail contact geometry. In the present case, $w_{30} = 0$, the sleeper span size $l_s = 600$ mm, and the running speeds of the wheel are, respectively, 22.22 and 33.33 m/s. When the wheel passages reach 10 times the fluctuation of the vertical load between the wheel and rail is shown in Fig. 20, and the maximum depth of wear shown in Fig. 21. It is noted that the fluctuation is caused by $\mathrm{FL}^*(x_p)$ and the wear accumulation after 10 passages of the wheel. Curves 1 and 2 stand for the two cases, in which the rolling speeds of the wheel are respectively, 22.22 and 33.33 m/s. Figs. 20 and 21 present that (1) ΔP and the wear amount in the second half of each sleeper span are larger than those in the first half span, the maximum of ΔP and the wear amount do not appear above the sleeper. The higher the running speed, and the larger ΔP is and the more serious the wear. The position with the larger ΔP and the larger wear amount have a tendency to move to the mid-span with an increase of the running speed. It is noted that the initial stages of the curves in Figs. 20 and 21 are in disorder since their oscillation at high frequencies is caused by the end condition of the calculation wear which does not exist in practice. So the situation occurring at the initial stage of

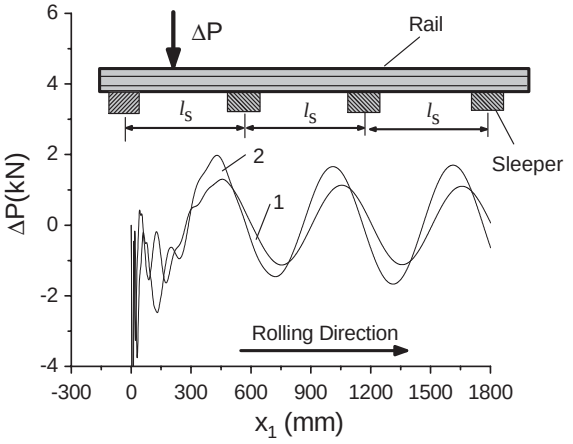

Fig. 20. Fluctuation of vertical load after the wheel passages of 10.

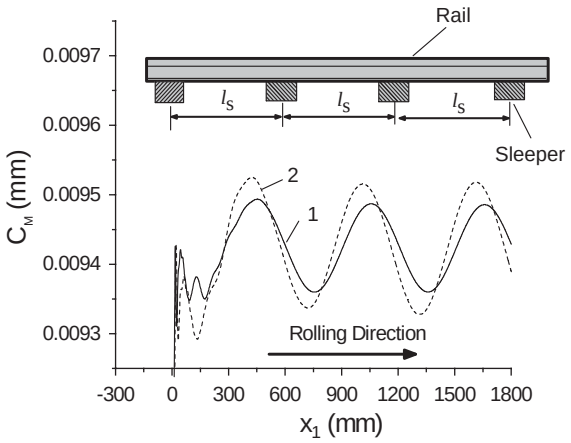

Fig. 21. Maximum depth of corrugation after the wheel passages of 10.

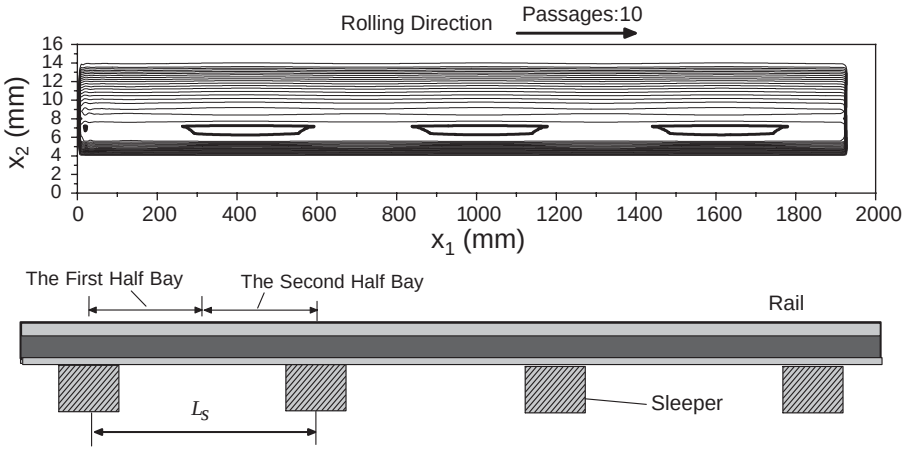

Fig. 22. Pattern of corrugation caused by sleeper pitch after the wheel passages of 10.

the curves should be not cared much. Fig. 22 indicates the pattern of the corrugation caused by the sleeper pitch after the wheel passages of 10 at speed of 33.33 m/s. The analysis of the other cases was carried out, in which higher running speeds and larger static axle-loads are considered. Except for the situation in the initial stage, the vertical loads did not oscillate at higher frequencies than the passing frequency of the sleepers shown in Figs. 20 and 21. But such oscillation phenomena were present in the results in Refs. [11,16]. That is probably because the track model discussed in the present paper is not very reasonable and needs to be further improved. Especially the rail needs to be modeled with the finite element method. So the phenomenon of corrugation observed by Clark [17], namely a short pitch corrugation appearing in the second half of sleeper bay, cannot be reproduced with the present theoretical model for rail corrugation. It is assumed that $\mathrm{FL}^*(x_p)$ is modulated by an oscillated function with higher frequency, and it is formulated as

$$\widetilde{\mathrm{FL}} = \mathrm{FL}^*(x_p) \cdot [1 - \cos(2\pi f t)] = \mathrm{FL}^*(x_p) \cdot [1 - \cos(2\pi x_p/\lambda_0)]. \tag{24}$$

In formula (24) the frequency f is selected to equal 271 Hz, namely a natural frequency of the track, or the wavelength λ_0 selected as 81.9 mm which is obtained by dividing the running speed of 22.222 m/s by f. Actually $FL^*(x_p)$ is the vertical displacement of the rail caused by the discrete support of the rail by sleepers, which is one of the pinned–pinned modes of the rail in a sleeper span, and the oscillated function is used to model a vibration of the track at high frequencies, which are the natural frequencies of the track, or the higher pinned–pinned frequencies. After the wheel passages of 10 the vertical load fluctuation caused by $\widetilde{FL}$ is shown in Fig. 23 and its linear spectrum shown in Fig. 24. Figs. 23 and 24 indicate that the vertical load between the wheel and rail oscillates at two frequencies, 37 and 271 Hz, which are, respectively, the passing frequency of the sleepers and the natural frequency of the track. The amplitude of the oscillation at 271 Hz is much larger than that at 37 Hz, which is present in Fig. 24. Fig. 25 indicates the pattern of corrugation developed after the wheel passages of 20. In the second half of sleeper bay the depth

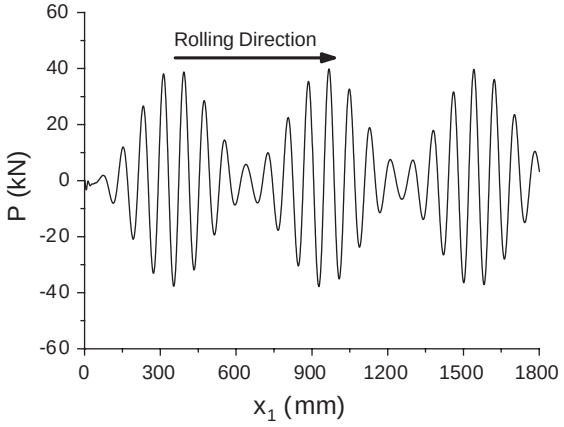

Fig. 23. Fluctuation of vertical load after the wheel passages of 10.

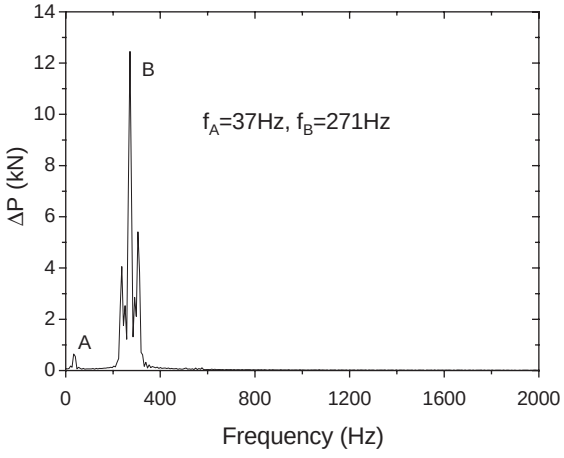

Fig. 24. Linear spectrum of vertical load fluctuation.

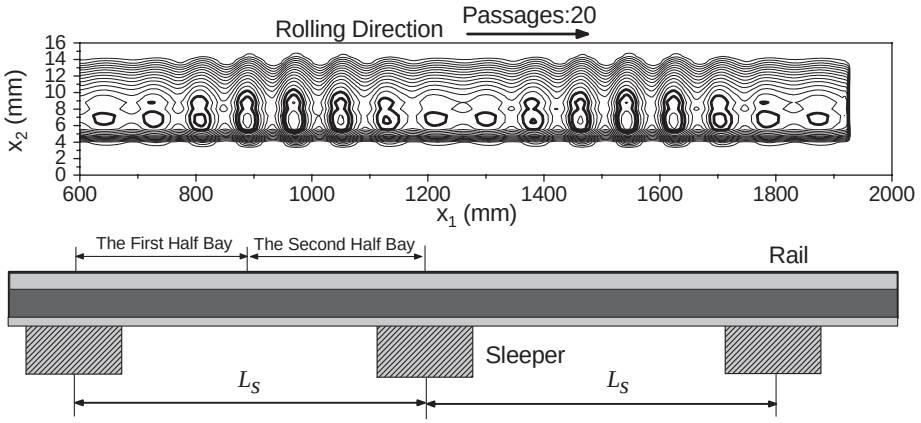

Fig. 25. Pattern of corrugation caused by sleeper pitch and high frequency oscillation after the wheel passages of 20.

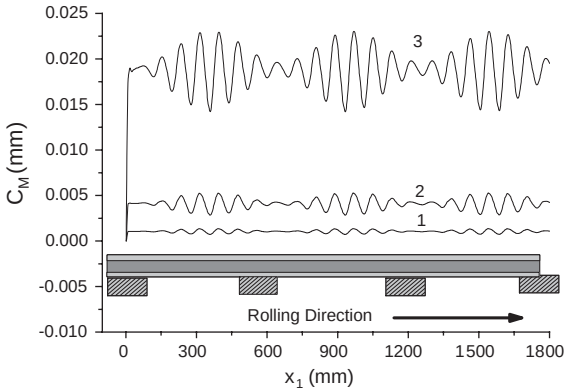

Fig. 26. Maximum depth of corrugation after different number of wheel passages.

of corrugation is larger than that in the first half of a sleeper span. The wavelengths in Fig. 25 depend on the frequency in oscillating function (24) and the natural frequencies of the track. In this case if the running speed or the sleeper pitch increases the formed corrugation with larger depth has a tendency to move to the midpoint of the sleep span, the corrugation phenomenon observed and analyzed by Vadillo and his colleagues could be reproduced with the numerical method, otherwise the corrugation with larger depth would move to the second half of the sleeper span or the position above the sleeper, which is just the situation of corrugation found by Clark. Now the open question left is how to develop a good model of the track to get a vertical displacement vibration function similar to formula (24). Probably it can be done by means of finite element method. So far it is not very difficult for us to do it but it takes long CPU time in the calculation.In addition if the number of the wheel passages is further increased and the plastic deformation of the material should be taken into account in the change of the rail profile, the pattern in Fig. 25 can spread evenly over the running surface of the rail in the longitudinal

direction of the track. It is because the rate of the plastic deformation at the position of the higher peaks is higher than that at the trough in the later stage of rail corrugation development. Fig. 26 illustrates the change of the maximum depth of time corrugation after different number of the wheel passages. Curves 1, 2 and 3 in Fig. 26 stand for the cases of the wheel passages of 1, 5 and 20, respectively. If the track considered is of a single track the initiation and development of the corrugation is approximately symmetrical in a sleeper span since the trains pass the track in the double directions.

5. Conclusions

The effect of track irregularities on the formation and evolution of rail corrugation is investigated in detail with numerical method when a railway vehicle is repeatedly curving. The irregularities considered in the present paper include initial running surface of rail with periodically varying and different wave length, stochastic roughness on the running surface, and uneven support stiffness of rail in the vertical direction due to discrete sleeper support. In the calculation we consider a combination of Kalker's rolling contact theory with non-Hertzian to be modified, a material wear model and a vertical dynamics model of railway vehicle coupled with a curved track. Also the influence of different speeds of wheelset curving through the irregularity track on rail corrugation is taken into account. The damage on the running surface of rail, due to an interaction of the wheel and rail, is only restricted to material wear mechanism of the material. Through the detailed numerical results the present paper comes to the following:

(1) For the existence of the initial corrugation of new curved rail with any fixing wavelength the depth from the peak to trough of it decreases gradually with an increase of wheel passage. The initial corrugation evolved has a tendency to move in the rolling direction.
(2) The amplitude of the initial stochastic roughness on the running surface of new curved rail is gradually leveled out but a corrugation with very small depth and a few fixed passing frequencies is initiated after the number of wheel passages. The passing frequencies are the same as some of the natural frequencies of the track.
(3) The discrete supports of rail by sleepers have a great influence on the formation of corrugation on a curved track under the condition of non-zero and steady creepages of wheels and rails. The larger the running speed is and the faster the increasing rate of the corrugation is. The corrugation developed has a tendency to move in the sleeper span in the longitudinal direction of the track with the change of the running speed. If the high frequencies of the track are excited by an interaction of the wheel and rail the short pitch corrugation can appear in the second half of each sleeper span or at the mid-span.

Acknowledgements

The current work has been supported by the Natural Science Foundation Committee of China that grants the key project: "Corrugation of Contact Surface of Wheel and Rail and Rolling

Contact Fatigue'' (59935100) to the State Key Laboratory of Traction Power, Southwest Jiaotong University. It has been also supported by the Foundation of Ph.D. Student Education of Education Ministry of China (20020613001) and the Special Foundation for Excellent Ph.D. Thesis.

The authors are grateful to the reviewers of the present paper for the suggestions of the paper revising. Special thanks are also due to the reviewers and the editors for their help in the improvement of our poor English writing.

References

[1] S.L. Grassie, Corrugation: variations on an enigma, *Railway Gazette International* 146 (7) (1990) 531–533.
[2] S.L. Grassie, J. Kalousek, Rail corrugation: characteristics, cause and treatments, *Proceedings of the Institution of Mechanical Engineers* 207 (1993) 57–68.
[3] Q.Y. Liu, X.S. Jin, X.Q. Wang, Z.R. Zhou, An investigation of rail corrugation in China, *Proceedings of the Fifth International Conference on Contact Mechanics and Wear of Rail/Wheel Systems*, Tokyo, July 2000, pp. 89–95.
[4] X.S. Jin, J.Y. Zhang, Z.F. Wen, L. Fu, Overview of phenomena of rolling contact fatigue wheel/rail, *Journal of Material Strength* 24 (2) (2002) 250–257 (in Chinese).
[5] Y. Sato, A. Matsumoto, K. Knothe, Review on rail corrugation studies, *Wear* 253 (1–2) (2002) 130–139.
[6] C.O. Frederick, A rail corrugation theory, *Proceedings of the Second International Symposium on Contact Mechanics and Wear of Rail/Wheel Systems*, Kingston/RI, July 1986, pp. 181–211.
[7] K. Hempelmann, Short pitch corrugation on railway rails—a linear model for prediction, *VDI Fortschritt-Berichte* 231 Reihe 12; Dusseldorf: VDI Verlag 1994.
[8] K. Knothe, B. Ripke, The effects of parameters of wheelset, track and running conditions on the growth rate of rail corrugation, *Vehicle System Dynamics (Supplement)* 18 (1989) 345–356.
[9] E. Tassilly, F. Vincent, A linear model for the corrugation of rails, *Journal of Sound and Vibration* 150 (1991) 25–45.
[10] K. Hempelmann, K. Knothe, An extended linear model for the prediction of short pitch corrugation, *Wear* 191 (1996) 161–169.
[11] J.J. Kalker, Considerations on rail corrugation, *Vehicle System Dynamics* 23 (1994) 3–28.
[12] A. Igeland, H. Ilias, Rail head corrugation growth predictions based non-linear high frequency vehicle/track interaction, *Wear* 213 (1997) 90–97.
[13] H. Ilias, The influence of railpad stiffness on wheelset/track interaction and corrugation growth, *Journal of Sound and Vibration* 227 (1999) 935–948.
[14] J.B. Nielsen, A nonlinear wear model, *ASME, Rail Transportation* RTD-13 (1997) 7–20.
[15] J.B. Nielsen, Evolution of rail corrugation predicted with a nonlinear wear model, *Journal of Sound and Vibration* 227 (1999) 915–933.
[16] R.A. Clarkr, P.A. Dean, J.A. Elkins, S.G. Newton, An investigation into the dynamic effects of railway vehicles running on corrugated rails, *Journal Mechanical Engineering Science* 24 (1982) 65–76.
[17] R.A. Clarkr, Slip-stick vibrations may hold the key to corrugation puzzle, *Railway Gazette International* 17 (1984) 531–533.
[18] E.G. Vadillo, J.A. Tarrago, G.G. Zubiaurre, C.A. Duque, Effect of sleeper distance on rail corrugation, *Wear* 217 (1998) 140–146.
[19] I. Gomez, E.G. Vadillo, An analytical approach to study a special case of booted sleeper track rail corrugation, *Wear* 251 (2001) 916–924.
[20] S. Müller, A linear wheel-track model to predict instability and short pitch corrugation, *Journal of Sound and Vibration* 227 (5) (1999) 899–913.
[21] S. Müller, A linear wheel–rail model to investigate stability and corrugation on straight track, *Wear* 243 (2000) 122–132.

[22] X. Jin, Study on Creep Theory of Wheel and Rail System, PhD Thesis, Southwest Jiaotong University, 1999 (in Chinese).
[23] W. Zhang, Dynamic Study Simulation of Railway Vehicles, PhD Thesis, Southwest Jiaotong University, 1996 (in Chinese).
[24] J.J. Kalker, *Three-Dimensional Elastic Bodies in Rolling Contact*, Kluwer Academic Publishers, The Netherlands, 1990, pp. 137–184.
[25] M. Hiensch, J.C.O. Nielson, E. Verherjen, Rail corrugation in The Netherlands—measurements and simulations, *Wear* 253 (2002) 140–149.
[26] P.J. Bolton, P. Clayton, I.J. Mcewan, Rolling–sliding wear damage in rail and tyre steels, *Wear* 120 (1987) 145–165.
[27] P. Clayton, Tribological aspects of wheel–rail contact: a review of recent experimental research, *Wear* 191 (1996) 170–183.
[28] K.Y. Wang, W.M. Zhai, C.B. Cai, The model of locomotive-track spatially coupled dynamics and its verification, *Journal of China Railway Society* 24 (4) (2002) 21–27 (in Chinese).
[29] I. Gomez, E.G. Vadillo, A linear model to explain short pitch corrugation on rails, *Wear* 255 (2001) 1127–1142.
[30] W.M. Zhai, Two simple fast integration methods for large-scale dynamic problems in engineering, *International Journal for Numerical Methods in Engineering* 39 (24) (1996) 4199–4214.
[31] W.M. Zhai, C.B. Cai, S.Z. Guo, Coupling model of vertical and lateral vehicle/track interactions, *Vehicle System Dynamics* 26 (1) (1996) 61–79.
[32] W.M. Zhai, C.B. Cai, Q.C. Wang, Z.W. Lu, X.S. Wu, Dynamic effect of vehicle on tracks in the case of raising train speed, *Journal of Rail and Rapid Transit* 215 (F2) (2001) 125–135.
[33] W.H. Zhang, J.Z. Chen, X.J. Wu, X.S. Jin, Wheel/rail adhesion and analysis by using full scale roller rig, *Wear* 253 (1–2) (2002) 82–88.